Ultraliser: a framework for creating multiscale, high-fidelity and geometrically realistic 3D models for *in silico* neuroscience

Marwan Abdellah[1], Juan José García Cantero[1], Nadir Román Guerrero[1], Alessandro Foni[1], Jay S. Coggan[1], Corrado Calì[2,4,5], Marco Agus[3,6], Eleftherios Zisis[1], Daniel Keller[1], Markus Hadwiger[3], Pierre J. Magistretti[2], Henry Markram[1] and Felix Schürmann[1*]

[1]Blue Brain Project (BBP)
École Polytecnique Fédérale de Lausanne (EPFL)
Geneva, Switzerland

[2]Biological and Environmental Sciences and Engineering Division
King Abdullah University of Science and Technology (KAUST)
Thuwal, Saudi Arabia

[3]Visual Computing Center
King Abdullah University of Science and Technology (KAUST)
Thuwal, Saudi Arabia

[4]Neuroscience Institute Cavalieri Ottolenghi (NICO)
Orbassano, Italy

[5]Department of Neuroscience, University of Torino
Torino, Italy

[6]College of Science and Engineering
Hamad Bin Khalifa University
Doha, Qatar

2022

[*]To whom correspondence should be addressed: marwan.abdellah@epfl.ch and felix.schuermann@epfl.ch

Abstract

ULTRALISER is a neuroscience-specific software framework capable of creating accurate and biologically realistic 3D models of complex neuroscientific structures at intracellular (e.g. mitochondria and endoplasmic reticula), cellular (e.g. neurons and glia) and even multicellular scales of resolution (e.g. cerebral vasculature and minicolumns). Resulting models are exported as triangulated surface meshes and annotated volumes for multiple applications in *in silico* neuroscience, allowing scalable supercomputer simulations that can unravel intricate cellular structure-function relationships. ULTRALISER implements a high performance and unconditionally robust voxelization engine adapted to create optimized watertight surface meshes and annotated voxel grids from arbitrary non-watertight triangular soups, digitized morphological skeletons or binary volumetric masks. The framework represents a major leap forward in simulation-based neuroscience, making it possible to employ high-resolution 3D structural models for quantification of surface areas and volumes, which are of the utmost importance for cellular and system simulations. The power of ULTRALISER is demonstrated with several use cases in which hundreds of models are created for potential application in diverse types of simulations. ULTRALISER is publicly released under the GNU GPL3 license on Github (BlueBrain/Ultraliser).

Keywords Ultrasturcture · mesh reconstruction · surface & solid voxelization · watertight · in silico · molecular simulations · reaction-diffusion simulations · optical imaging simulations · Ultraliser

Significance There is crystal clear evidence on the impact of cell shape on its signaling mechanisms. Structural models can therefore be insightful to realize the function; the more realistic the structure can be, the further we get insights into the function. Creating realistic structural models from existing ones is challenging, particularly when needed for detailed subcellular simulations. We present ULTRALISER, a neuroscience-dedicated framework capable of building these structural models with realistic and detailed cellular geometries that can be used for simulations.

1 Introduction

It has been more than a 100 years since Santiago Ramón y Cajal (1854–1934) commenced his pioneering quest to study the brain by elucidating its anatomical structures and establishing the neuron doctrine[1]. Nevertheless, and so far, our knowledge is still incomplete, particularly at cellular and synaptic levels-of-detail[2]. Even with the broad spectrum of research that followed Cajal's leading efforts, taking into account the vast amount of resulting data, it has been proven that conventional wet lab experiments alone are insufficient to unravel the underlying function of the brain[3]. The generation of massive amounts of experimental data in addition to the recent quantum leap in computing technologies have led to the renaissance of a complementary approach: simulation neuroscience[4]. Mathematical modeling, computer simulations and terabytes of structural data resulting from a myriad diversity of experiments are being successfully consolidated — with this approach we can test our hypotheses and predict the quantitative behavior of complex biological processes[5].

Data-driven models integrated with systematic computational methods can dramatically increase efficiency, efficacy and reliability of simulations[6], particularly when our experimental knowledge is fragmented[5]. An important question is whether we can reuse existing structural data to synthesize detailed, multiscale and biologically plausible three-dimensional (3D) models that can be integrated into simulation contexts to gain insights into the cellular function. The interdependency of structure and function produces a kind of metaplasticity[7] that requires performing simulations within geometrically realistic subdomains at ultrastructural resolutions in which molecular reactions can be contained[8].

Structural neuroscientific datasets are either acquired from a wide spectrum of imaging modalities, such as imaging scanners and microscopes[9–11] or digitally synthesized in supercomputer simulations to yield similar structural characteristics of biological counterparts[12–15]. 3D models of structural data (on the scale of 100 nm - 1 mm) can be classified according to their digital representations into four principal formats: morphology skeletons, surface meshes, volumetric meshes and volumetric grids. Each representation (**Supplementary Fig. S1**) is convenient for a specific category of simulation.

Morphology skeletons are point-and-diameter descriptions of either acyclic or cyclic graphs that can model connectivity of neuronal arborizations[16], astrocytic processes[15] and dense vascular networks[17,18]. Aside from their usage for topological and visual analysis[19], these morphologies are used to conduct one-dimensional (1D) compartmental simulations. Neuronal and glial morphologies are used in NEURON[20] (neuron.yale.edu) to simulate electrophysiology based on Hodgkin-Huxely ion channel formalism[21], and vascular morphologies are used to simulate blood flow in cerebral vasculature[22,23].

Surface meshes are sets of vertices, edges and facets (ideally triangles) that can define the boundaries of 3D structures, such as cellular membranes of neurons[24] and astrocytes[25] and tubular membranes of blood vessels[26]. These meshes, if watertight, are extensively used in particle-based stochastic molecular simulations, for example with the MCell simulator[27,28](mcell.org).

Volumetric meshes are derived from their surface counterparts to model their interior volume with convenient discretization, for example, with tetrahedral[29] or hexahedral[30] subdomains. Such meshes are primar-

ily used in reaction-diffusion simulations, for example with STEPs[31] (steps.sourceforge.net) or Smoldyn[32–34] (www.smoldyn.org).

Cartesian volumetric grids use, alternatively, cubic discretization to model the interior volume, in which we can account for the variations in optical properties of different regions of the tissue to simulate its interaction with light[35,36].

Generally, the same 3D model can be converted from one format to another to be used in hybrid or multimodal simulations; however, the principal format with which a given 3D model can be restructured into any other format is a surface mesh that must be watertight (**Supplementary Figs. S1b, S2**). For instance, the generation of a volumetric mesh from a surface input —using TetGen[37], QuarTet[38], GMsh[39] or CGAL[40]— requires the surface mesh to be watertight. TetWild can tetrahedralize non-watertight meshes, but it has limited performance[29] and fails to handle complex biological models with realistic geometries[41].

Moreover, accurate skeletonization of cerebral vasculature from microscopy stacks requires multimodal algorithms that combine an input volume with its corresponding watertight mesh to create a morphological representation of the network[42–44]. Therefore, to automate and systematize simulation workflows, watertightness is essential, not only for the simulation per se, but also for data conversion from one representation to another.

On one level, and as a consequence of the segmentation challenges of electron microscopy (EM) volumes, existing 3D mesh models of cellular and subcellular brain structures are expected to be fragmented and non-watertight. This applies to manually segmented neuropil structures[11] or even those segmented with state-of-the-art deep neural networks[45]. Machine learning (ML) has helped automating the process allowing to generate a massive amount of neuro-glia-vasculature (NGV) reconstructions that are disseminated online as demonstrated by several research programs such as MICrONS Explorer[46], FAFB-FFN1[47], and FlyEM Hemibrain[48]. Nevertheless, the majority of the resulting reconstructions requires many person-years of effort for proofreading. Online collaborative efforts are introduced to accelerate the process[49], which could be effective in resolving fragmentation artifacts, but watertightness remains lacking.

On another level, there is a huge diversity of NGV morphological models that have been released publicly to central databases, for instance, NeuroMorpho.Org[16] and Brain Vasculature (BraVa)[18]. These models are only appropriate for conducting 1D compartmental simulations; there are no existing frameworks that can convert them, taking into consideration their structural artifacts, into watertight mesh models for applications in other types of simulations. The key question ther efore is, given an input 3D model in any of aforementioned formats, can we reconstruct it in another format that can be systematically plugged into simulation environments for *in silico* experimentation? We present Ultraliser to address this challenge.

2 Results

2.1 Ultraliser

Ultraliser is a neuroscience-specific framework capable of creating multiscale (from the subcellular scale up to mesoscale circuits) and high fidelity 3D models of neuroscientific datasets that can be integrated in the context

of simulation-based experiments, aiming to understand the function. Ultraliser is consistent and unconditionally robust, as it can systematically build adaptively optimized watertight triangular meshes and large-scale annotated volumes from input data models with multiple formats including: (i) ill-conditioned, fragmented and self-intersecting polygonal meshes with irregular topologies, (ii) cyclic and acyclic morphological graphs, (iii) gray-scale volumetric stacks with user-specified isovalues, (iv) binary volume masks segmented from microscopy stacks, and (v) tetrahedral volumetric meshes.

Contrary to traditional remeshing applications that use geometry-based methods[50] to repair the geometric topology of non-watertight meshes, the core engine of Ultraliser is designed based on efficient voxelization kernels that create intermediate high resolution proxy volumes, with which we can extract continuous surface meshes that are adaptively optimized and watertight, refer to **Figure 1** and **Supplementary Figure S2**. The core library of Ultraliser is exploited to develop several applications that can be part of a large-scale software ecosystem for establishing fully automated neuroscientific pipelines involving multimodal simulation systems. The current version of Ultraliser integrates the following applications:

1. ultraMesh2Mesh, restructures an input polygonal surface mesh with a set of unorganized triangles with no defined connectivity—i.e. a triangle soup—into a smooth, optimized, two-manifold and watertight triangular surface mesh.

2. ultraMeshes2Mesh, a similar application to ultraMesh2Mesh, but it produces a single output watertight mesh from a list of non-watertight input meshes that have existing spatial relationship.

3. ultraMesh2Volume, reconstructs 1-bit (one bit per voxel) and 8-bit (one byte per voxel) volumes from an input mesh that is not necessarily watertight and might have severe geometric deficits including self-intersecting facets, fragmented partitions and even floating vertices.

4. ultraVolume2Mesh, generates a watertight surface mesh from an input 8-bit gray-scale volume stack. The surface of the resulting mesh is established based on a user-specified isovalue or range of isovalues.

5. ultraMask2Mesh, a similar application to ultraVolume2Mesh, but it takes an input binary mask that is typically segmented from microscopy stacks, where the isosurface is already reconstructed as a set of voxels.

6. ultraNeuroMorpho2Mesh, converts an input acyclic graph representing a neuronal morphology skeleton into an optimized and continuous membrane with a biologically realistic 3D somatic profile reconstructed on a physically plausible basis. Spines can be also integrated along the dendritic surface if the morphology is reconstructed in a digital microcircuit[2], where synaptic locations are determined.

7. ultraAstroMorpho2Mesh, converts an input astrocytic morphology containing branching processes and endfeet surfaces into an optimized and continuous membrane surface.

8. ultraVessMorpho2Mesh, converts an input cyclic graph representing a large-scale vascular network into an optimized, watertight and multi-partitioned mesh model with accurate branching geometries.

9. ultraCircuit2Volume, takes an input microcircuit and a configuration file, and produces a volumetric tissue model that is tagged with multiple optical properties. The configuration file describes the annotation details of the circuit.

10. ultraTet2Surface, takes an input tetrahedral volumetric mesh and creates a corresponding watertight triangular surface mesh.

In the following sections, we demonstrate the significance of Ultraliser for *in silico* neuroscience taking into account several use cases that involve multiple types of input structural data including: non-watertight surface meshes of cellular and subcellular structures segmented from EM volumes and NGV (neuronal, astrocytic and vascular) morphologies that are either segmented from optical microscopy stacks or generated synthetically.

2.2 Remeshing cellular and subcellular structures of the NGV ensemble[51]

In the context of a recent collaboration between EPFL and KAUST, we developed a multi-stage framework (imaging, segmentation, modeling, simulation and visualization) to re-create the NGV ensemble *in silico*[51]. This framework aims to advance our understanding of the substantial role of cytoscale structures and functions in controlling brain energy metabolism. Our fundamental objective is to digitally reconstruct 3D structural models of NGV structures with realistic geometries to fuel detailed subcellular simulations[52,53], allowing us to investigate the biochemical and biophysical properties of oligocellular networks[54]. Realizing the objectives of this framework, however, has been impeded by the lack of availability of topologically accurate watertight meshes with which we can conduct the simulations or even skeletonize the meshes extracted in the segmentation stage (**Fig. 2a**).

We acquired a 750,000 cubic micron volume from layer IV of the somatosensory cortex of a two-week-old rat. Within this volume, a total of 186 structures were labeled, segmented, and classified into (i) cellular structures including: astrocytes, neurons, microglia, pericytes and oligodendrocytes, (ii) subcellular structures including: nuclei, mitochondira and endoplasmic reticula (ER), (iii) other fragmented structures including a few blood vessel segments and a group of myelinated axons and (iv) other non-identifiable structures. From this collection, the following *complete* structures — that are of central significance to our modeling objectives — were segmented: four astrocytes, four neurons, four microglia, four pericytes and a single oligodendrocyte in addition to the mitochondria of all the cells and the ER of the astrocytes (**Supplementary Section 3**).

A surface mesh model corresponding to each structure is exported into a Wavefront OBJ file for qualitative and quantitative analysis (**Supplementary Tables S1** and **S2**). From those 17 cells and their subcellular structures, only the meshes of three pericytes and astrocytic ER were verified to be watertight. Meshes of the remaining cells were confirmed to be non-watertight; containing thousands of non-manifold edges and vertices in addition to tens of self-intersecting polygons.

We then re-meshed all the cellular and subcellular meshes using ultraMesh2Mesh to reconstruct corresponding watertight manifolds that are accurate and geometrically optimized (Methods). Geometric accuracy, tessellation and topology of the resulting meshes are subject to two principal parameters: voxelization resolution and number of optimization iterations. Resolution is defined by the number of voxels per micron used to

rasterize the input mesh. Geometric accuracy is primarily measured by the Hausdorff distance and difference in volume between the input and output meshes.

To estimate the optimum values of these two parameters, we constructed five analysis matrices for an exemplar mesh (Astrocyte 4, shown in **Fig. 2b**) in which we can apply those optimum values to other cellular meshes in the block. **Figure 2c** illustrates four quantitative matrices showing the effect of varying the two principal parameters on the Hausdorff distance, number of vertices, surface area and volume of the output mesh. **Figure 2d** shows the effect of using one, five and ten optimization iterations on the tessellation and topology of the resulting mesh. The full analysis matrix is shown in **Supplementary Figure S4**. From this analysis, the optimum values were estimated to be five voxels per micron and five optimization iterations. Those values are then used to re-mesh all the cellular meshes in the block. **Supplementary Figures S5 - S26** (**Table S4**) reveal detailed quantitative, qualitative and visual comparisons (the results for Astrocyte 2 are shown in **Figure 2e**) between the input and output meshes of the complete cellular structures shown in **Figure 2a**.

Subcellular meshes were re-meshed with higher voxelization resolution (10 voxels per micron) to ensure resolving their fragmented and minuscule segments. Complete comparative analysis of the subcellular meshes is shown in **Supplementary Figures S29 - S53** (**Table S5**).

Resulting astrocytic meshes were therefore applicable for skeletonization, with which we have successfully developed a novel pipeline to synthesize a digital reconstruction of the NGV ensemble at micrometer anatomical resolution[15]. Moreover, all the resulting meshes were tetrahedralized using TetGen[37] and Gmsh[39] to create corresponding volume, or simulation-ready, meshes for STEPs[31] simulations to accomplish the objectives of the collaboration. Simulation results are beyond the scope of this sequel.

2.3 Remeshing poorly segmented meshes with fragmented partitions and slicing artifacts

Dense reconstructions of brain circuits are made available with volume EM and advanced ML-based segmentation solutions, allowing us to render hundreds of thousands of cortical structures — including complete cells, cell parts, cytoplasmic organelles and blood vessels — that are shared[55] and made freely available online[47,48,56,57]. A decent amount of the segmented structures are proofread to resolve false-split (fragmentation) and false-merge (connectivity) errors. Nevertheless, pipelines involved in the segmentation process yield triangular mesh models characterized by sharp features, rough surfaces and high tessellation rates, leading to triangle soups with giant numbers of geometric deficits. The meshes might have large discontinued partitions with overlapping geometries (**Figs. 3a, b, f**), gaps (**Fig. 3j**) and tiny disconnected fragments (**Supplementary Fig. S75**) due to common slicing and misalignment artifacts[58]. Those poorly reconstructed and fragmented meshes cannot be effectively repaired — or remeshed to produce watertight counterparts — relying on geometric-based solutions[50]. Thanks to its voxelization engine, Ultraliser can transparently handle these deficits and build a continuous, adaptively tessellated and high resolution manifold of the entire structure with superior topology.

To accomplish this objective, we used ultraMesh2Mesh, with which the polygons of an input surface mesh are independently rasterized into a volume grid, where self-intersecting and duplicate facets are implicitly eliminated; they are rasterized to the same voxel or a neighboring one. This grid is then processed by isosurface

extraction kernels to produce an intermediate highly tessellated surface, which is smoothed, adaptively optimized and finally verified to be watertight (Methods). **Figure 3** demonstrates how effective ULTRALISER can be in processing an exemplar mesh —segmented from layer II/III of the visual cortex of a young rat— with thousands of mesh partitions, self-intersections and other geometric artifacts. **Supplementary Figures S55 - S74** show comparative remeshing results for a small subset of meshes of pyramidal neurons (the full block is shown in **Supplementary Fig. S54**) that were publicly provided by MICrONS Explorer[46]. All the resulting meshes are watertight and have a single mesh partition with a continuous manifold.

Segmented meshes suffering from slicing or alignment artifacts are, in certain cases, characterized by thin gaps across their surfaces. Such gaps lead to surface discontinuity (**Fig. 3j**) or disconnected fragments of the mesh (shown in red in **Supplementary Fig. S75**). Those gaps cannot be easily detected and might require advanced and computationally intensive ML-based algorithms to identify and repair them. In our implementation, we extended the voxelization stage and integrated a 3-way solid voxelization algorithm, that is seamlessly taking into account repairing those gaps, in which the interiors bounded by cell membranes are voxelized along each axis independently and then merged into a single volume (Methods). **Figures 3k, l, m** illustrate the results of remeshing a pyramidal neuron mesh with three obvious slicing artifacts (two of them exist on the soma and one is located along a dendritic branch) into a continuous surface mesh at three different voxelization resolutions. **Supplementary Figure S75** illustrates a side-by-side comparison between an input mesh with several artifacts and the resulting one from ULTRASMESH2MESH, in which all the gaps are filled to connect the disconnected fragments to the surface of the mesh to produce a continuous surface.

2.4 Generating biologically realistic neuronal meshes from digitized morphologies

There is a huge diversity of neuronal morphologies (mainly in SWC format) that is routinely used for simulating electrical activity in NEURON[20]. Such diversity can be a significant resource for performing meso-scale hybrid simulations combining electrophysiology with intracellular calcium dynamics simultaneously[59]. However, this objective entails the development of a robust technique that can construct biologically detailed and watertight neuronal mesh models consistent with their morphological counterparts. Several applications were developed to create neuronal surface meshes from their corresponding morphologies (summarized in **Supplementary Table S7**). The majority was focused on building low-tessellated, non-watertight and visually appealing mesh models that can be quickly generated and efficiently used for visualization or in visual analytics[19,24,60–62]. Only a few ones addressed the watertightness challenge, however, using simplified geometries and without support to integrate spine models[63,64]. We therefore implemented an application (ULTRANEUROMORPHO2MESH) capable of consolidating neuronal meshes combining both features, biological realism and watertightness, irrespective to the conditions or topology of the input morphology.

To create an integrated mesh model of a spiny neuronal morphology, our implementation addressed four principal challenges: (i) creating a plausible 3D somatic surface that can simulate the biological growth of the soma relying merely on the initial segments of the neurites, (ii) creating neuritic arborization membranes with non-overlapping geometries around their bifurcation points, irrespective to their branching angles, (iii) inte-

grating realistic spine models along the membranes of their dendritic branches, and finally (iv) optimization and watertightness verification (Methods).

Digitized neuronal morphologies are composed of three distinct structural components: somata, neurities and dendritic spines (**Supplementary Fig. S76**). Somata are typically approximated with geometric primitives, mainly a sphere[63], whose radius is computed based on the relative locations of the initial segments of each neurite, or in some cases, cylinders[65]. Advanced traces digitize the soma into a two-dimensional (2D) contour representing its projection along the optical axis. To reconstruct a plausible 3D somatic profile, we apply the finite element method (FEM) approach[66] to deform a volumetric model of an elastic sphere by pulling towards each neurite in the morphology. This approach preserves the initial volume of the sphere, resulting into more realistic somatic surface (**Fig. 4a**). Neurites are represented by directed acyclic graphs (DAGs) as a set of interconnected nodes, each of which defines a 3D Cartesian position and radius (**Fig. 4b**), with which we can reproduce cross-sectional variations and orientation of each segment in the morphology. A depth-first scheme is used to construct a set of connected paths from the root node (or the soma) to the terminal ones. For each path, a cross-sectional geometry is created as an independent proxy mesh (**Fig. 4c**) (Methods). The integration of the spines along dendritic membranes is optional; spines are not comprised by default within the morphological descriptions of individual neurons loaded from SWC files. Spiny neurons are modeled after circuit building[2], where we can localize synapses and characterize their spine attributes. We designed a set of realistic spine geometries (**Supplementary Fig. S79**) based on a few reconstructions of interneurons segmented from the somatosensory cortex[11]. All the proxy meshes — of the soma, neurites and spines — are agglomerated and rasterized in parallel to create a corresponding solid volume, with which the final mesh is generated (Methods). **Figure 4** illustrates the steps of building a mesh model of a spiny neuron from its morphology skeleton. The resulting mesh is shown in detail in **Supplementary Figure S81**. Our implementation has been tested with a group of 25 neurons with various morphological types[67]. The morphology files and resulting meshes are available in the Supplementary Data.

2.5 Generating astroglial meshes from complete synthetic morphologies

Complete astrocytic morphologies with endfeet reconstructions are sparse. NeuroMorpho.Org has ∼3,500 astrocytes , but none of them contains any endfeet descriptions; only the arborizations of perisynaptic and perivascular processes. Based on a few reconstructions of complete astroglial morphologies[11], we presented in a recent study[15] an effective method to synthesize biologically inspired, and complete, astrocytic morphologies including endfeet patches (the skeleton of an astroglial morphology is shown **Supplementary Fig. S77**). The objective of the study is to allow the creation of a huge diversity of astrocytic morphologies that can be used to understand their structure-function relationship using molecular simulations. We therefore complemented this effort and integrated a specific application (ultraAstroMorpho2Mesh) to create simulation-ready astrocytic meshes from their morphological counterparts. The mesh generation algorithm is similar to that used to create neuronal meshes, but in addition, endfeet proxy geometries are created using implicit surface modeling (Methods). **Supplementary Figure S82** illustrates the results for reconstructing a watertight astrocytic

mesh that is consistent with its morphological description. We also tested the implementation with a group of 25 astrocytes sampled from different cortical regions and created corresponding watertight manifolds. The morphologies and resulting meshes are available in the Supplementary Data.

2.6 Generating continuous cellular meshes from fragmented components

We extended the re-meshing pipeline and integrated another application (ULTRAMESHES2MESH) that agglomerates a list of fragmented meshes —that are spatially overlapping— into a single and continuous watertight mesh. This extension, however seamless, enables the reconstruction of ultrarealistic cellular models based on existing meshing implementations (**Supplementary Table S7**), in which we can assemble 3D mesh models of different cellular components generated independently by multiple third-party applications into a single watertight mesh with continuous surface (Methods). For instance, ULTRANEUROMORPHO2MESH uses the FEM to reconstruct a plausible 3D surface of the soma, but meanwhile, there are other advanced implementations that use Hooke's law and mass-spring models to reconstruct 3D somatic profiles with more realistic shapes, which could ultimately improve the realism of resulting neuronal meshes. This can be demonstrated with the Soma Reconstruction Toolbox in NeuroMorphoVis[19], where users can fine tune the parameters of the soma reconstruction algorithm and validate the resulting profile with respect to a segmented ground-truth mesh. **Supplementary Figure S81** provides an example of creating a watertight mesh of a spiny neuron from a set of input meshes, each represents a single component of the neuron (soma, arbor, or even a spine). ULTRAMESHES2MESH can therefore be seen as a complementary or post-processing application that can ensure the watertightness of resulting mesh models of NGV cellular structures created by other software applications.

2.7 Generating vasculature meshes from corresponding graph networks

Another application is developed to create 'multi-partitioned' watertight mesh models of large-scale cerebral vascular networks. This application is intended to confront the rising trend to automate the reconstruction of accurate 3D models of brain vasculature, with which we can analyze their structural angioarchitecture and characterize their dynamic behavior[17,68]. The networks are typically segmented into vectorized graphs, i.e. centerlines with point-and-diameter representations (the structure of a vascular morphology graph is shown in **Supplementary Fig. S78**). Those graphs are becoming imperative for performing vascular simulations, whether used in vectorized format in 1D compartmental simulations or being converted into alternative formats, for example, into tetrahedral meshes that can be applied in reaction-diffusion simulations. Such simulations pave the way to understand how our brains meet the energy demands of neuronal computations. Nevertheless, creating such 'simulation-ready' vascular models from segmented data is challenging.

The first challenge is the fragmentation of the network. Even with current state-of-the-art imaging and segmentation protocols, it is near impossible to reconstruct a full – and accurate – high resolution cerebral vascular network segmented into a single and connected graph[69]. Resulting graphs are typically composed of multiple disconnected partitions, which complicates the creation of watertight meshes if the partitions are self-intersecting. The second challenge is the scale of segmented networks, which has been exponentially growing

due to the recent advances in lightsheet imaging and Clarity[70,71], allowing to create whole-brain vascular maps down to capillary level[72]. The third challenge is the segmentation quality of the vessel network; in particular for small vessels, the quality is not optimum, and the resulting skeletons might have severe topological artifacts around branching terminals. Therefore, typical meshing algorithms of branching structures would fail to build watertight meshes of such complex geometries.

There are plenty of tools that can be used to visualize the graphs, but only a few are capable of visualizing large-scale graphs[26,73]. Some tools[26,62] can also create surface meshes from their corresponding morphologies, but usually the results are not watertight, particularly for dense graphs. To fill this gap, we designed ULTRAVESSMORPHO2MESH, a vasculature-specific application that can efficiently convert large-scale networks of vascular morphologies into multi-partitioned and adaptively optimized watertight meshes with smooth branching geometries. Our algorithm handles an input graph as a linear list of sections without the necessity to have predefined connectivity information. Initially, the morphology skeleton is analyzed, where high frequency variations in cross-sectional radii are filtered and short sections are eliminated (**Fig. 5b**). Each section in the graph is independently converted into a proxy mesh. However, and to guarantee the connectivity of branches along the surface of the final mesh, we add multiple sphere meshes (icospheres) at both terminals of the section. All the proxy meshes are then rasterized and converted into a solid volume, with which the final mesh is generated (Methods).

Due to the cyclic nature of vascular graphs, there is a high possibility that our slice-based solid voxelization algorithm will fail. We therefore use 3-way solid voxelization instead of 1-way voxelization, in which the flood-filling algorithm is applied on every principal axis independently. Prior to the optimization stage, the different partitions in the polygonized mesh object are split and optimized individually. After optimization, these partitions are regrouped again in a single mesh object (Methods). **Figure 5** depicts the stages of processing a fragmented vascular network towards reconstructing a high fidelity watertight surface mesh with multiple partitions. **Supplementary Figure S81** shows the results of converting a more complex vascular network into a watertight mesh with ULTRAVESSMORPHO2MESH and ultimately into a tetrahedral one using TETGEN[37].

2.8 Generating annotated 3D tissue volumes from digital circuits

We also extended ULTRALISER to create annotated voxel-based tissue models from surface meshes of neuronal morphologies. Voxel-based models are becoming essential, not only for visual analytics, but also for performing *in silico* optical imaging experiments that simulate light interaction with brain tissue using physically plausible Monte Carlo visualization[10]. Simulation applicability and even its accuracy are subject to two factors. First, the derivation of advanced mathematical formalism of the radiative transfer equation (RTE) that could account for absorption, scattering and, in certain cases, fluorescence. Second, the existence of biologically realistic 3D models that account for (i) the optical properties of brain tissue across its different regions at microscopic levels and (ii) the spectral properties of fluorescent dyes used in wet lab experiments for cell labeling.

What is missing then? RTE was extended to model light interaction with low- and high-scattering fluorescent participating media[35,74], recent experiments were able to build accurate 3D brain atlases mapping the

different optical properties of the tissue[75], and fluorescence databases are available online, where spectral properties of common fluorescent dyes are provided. The only missing element is a robust application capable of creating detailed biologically and optically accurate volume models of cortical circuits. To address this issue, we implemented ultraCircuit2Volume.

Our implementation uses the information retrieved from the circuits that are digitally reconstructed by the Blue Brain Project[2,67]. These circuits identify neuron types, their coordinates and orientation. Starting from raw morphologies, corresponding surface meshes are generated either with Ultraliser directly or relying on third-party applications, such as NeuroMorphoVis[19](github.com/BlueBrain/NeuroMorphoVis). Meshes are then rasterized in voxel grids, where each voxel is annotated with location-specific optical properties. In case of fluorescence, voxels corresponding to intracellular spaces are annotated with the spectral parameters of fluorescent dyes (Methods). The resulting volumes are used with recently developed *in silico* imaging simulators[10] to create synthetic optical sections of cortical tissue models, on physically plausible basis (showin in **Fig. 6** and **Supplementary Fig. S85**).

3 Conclusion

Biologically realistic simulations are indispensable for revealing the structure-function relationships within and among brain cells. Driven by a quantum leap in computing technologies, *in silico* brain research is complementing *in vivo* and *in vitro* methods. Meanwhile, advances in imaging technologies and automated ML-based segmentation algorithms are boosting the creation of detailed and anatomically realistic 3D neuroscientific models that are fueling simulation-based research. The goal of Ultraliser is to provide a systematic and robust framework for creating accurate watertight meshes and high resolution annotated volumes of 3D brain structures that can be integrated in multimodal supercomputer simulations. On one level, Ultraliser unconditionally rectifies non-watertight mesh models that cannot be repaired with existing meshing solutions. On another level, it has native support to create ultrarealistic watertight meshes and annotated volumes of NGV models from their morphological descriptions. The framework has a modular and extensible architecture, making it possible to integrate further relevant applications that are of paramount importance in structural systems neuroscience.

Data sources

Cellular and subcellular NGV meshes segmented from the volume shown in **Figure 2** are provided by the collaborating co-authors affiliated with KAUST. Neuronal meshes shown in **Figure 3** and **Supplementary Figures S55 - S75** are publicly available from the MICrONS Explorer program. Neuronal morphologies shown in **Figure 4** and **Supplementary Figure S81** are publicly available from NeuroMorpho.Org. Astrocytic morphologies (**Supplementary Figure S82**) are provided by Eleftherios Zisis[15]. Vascular morphologies (rat's cerebral microvasculature) shown in **Figure 5** and **Supplementary Figure S83** are courtesy of Bruno Weber[22], University of Zürich (UZH).

Supplementary Data

Supplementary Data 1 contains the input (non-watertight) surface meshes of the block (shown in **Figure 2a**) reconstructed within the context of the EPFL-KAUST collaboration, and the corresponding output (watertight) meshes generated by ULTRALISER. **Supplementary Data 2** contains a set of 20 non-watertight meshes that were randomly selected from the block shown in **Supplementary Figure S54** and another set of the their watertight counterparts. The input meshes were downloaded from the MICrONS Explorer program. **Supplementary Data 3** contains a set of 25 neuronal morphologies with different morphological types and their corresponding watertight meshes. **Supplementary Data 4** contains a set of 25 synthetic astroglial morphologies[15] and their corresponding watertight meshes. **Supplementary Data 5** contains the vascular morphology (shown in **Supplementary Fig. S83**) and a corresponding multi-partitioned watertight mesh in addition to a tetrahedral mesh created with TetGen. Neuronal, astrocytic and vascular morphologies are stored in SWC, H5 and VMV file formats respectively. SWC and VMV formats are publicly available online. The H5 files of the complete astrocyte cells can be made available from corresponding authors upon request. All the meshes are stored in Wavefront OBJ files. All input and generated datasets are currently available upon request. The datasets will be publicaly available on Zenodo after the publication of this manuscript.

Software availability

Ultraliser is developed entirely in C++. The data-parallel sections of the code are parallelized using OpenMP[76]. The code is released to public as an open-source software (OSS) in accordance with the regulations of the Blue Brain Project, École polytechnique fédérale de Lausanne (EPFL) for open sourcing under the GNU GPL3 license. The code is freely available online at https://github.com/BlueBrain/Ultraliser. The version of the code used to create all the results demonstrated in this study is available in the **Supplementary Software**.

Methods

Methods and any associated references are available in the attached **Methods Document**.

Acknowledgments

We thank Grigori Chevtchenko and Samuel Lapere for the impactful discussions on watertight meshing, Pawel Podhajski on technical assistance to deploy the software on Blue Brain 5. We also thank Karin Holm and Judit Planas for their valuable comments on the manuscript. We acknowledge the artistic touch of Elvis Boci to improve the quality of figures.

Funding

This study was supported by funding to the Blue Brain Project, a research center of the École Polytechnique Fédérale de Lausanne (EPFL), from the Swiss government's ETH Board of the Swiss Federal Institutes of Technology. This publication is based upon work supported by the King Abdullah University of Science and Technology (KAUST) Office of Sponsored Research (OSR) under Award No. OSR-2017-CRG6-3438.

Authors contributions

M.A. and F.S. co-conceived the study. M.A., M.H., H.M, P.M., F.S. co-led the study. M.A. designed and implemented the framework, reconstructed and analyzed the resulting models and wrote the manuscript with input and critique from all authors. JJ.G.C. implemented the neuronal mesh reconstruction algorithm with FEM simulation, implemented the astrocytic endfeet proxy mesh reconstruction using implicit surfaces and contributed to the manuscript. N.R.G implemented the surface smoothing filters and contributed to the manuscript. A.F. implemented the morphology and mesh analysis code and provided technical assistance to load the H5 meshes downloaded from MICrONS Explorer. JS.C. contributed to the simulation discussions and the manuscript. C.C. reconstructed the NGV datasets within the EPFL-KAUST collaboration, analyzed them and contributed to the manuscript. M.Ag. contributed to the meshing discussions. E.Z. processed and provided the vasculature morphologies based on the original data set that was reconstructed by Bruno Weber (UZH), created the synthetic astrocytic morphologies and provided assistance to load them in Python. D.K. contributed to the discussions on the simulation requirements and the watertight meshing performance. All authors reviewed the manuscript.

Competing financial interests

The authors declare no competing financial interests.

Additional information

Supplementary information is available in the attached **Supplementary Document**.

Correspondence and requests for materials should be addressed to M.A and F.S.

References

[1] Santiago Ramón y Cajal. *Histologie du système nerveux de l'homme & des vertébrés: Cervelet, cerveau moyen, rétine, couche optique, corps strié, écorce cérébrale générale & régionale, grand sympathique*. Vol. 2. A. Maloine, 1911.

[2] Henry Markram et al. "Reconstruction and simulation of neocortical microcircuitry". In: *Cell* 163.2 (2015), pp. 456–492. DOI: 10.1016/j.cell.2015.09.029.

[3] Barbara Di Ventura et al. "From in vivo to in silico biology and back". In: *Nature* 443.7111 (2006), pp. 527–533. DOI: 10.1038/nature05127.

[4] Henry Markram. "The Blue Brain Project". In: *Nature Reviews Neuroscience* 7.2 (2006), pp. 153–160. DOI: 10.1038/nrn1848.

[5] Wulfram Gerstner, Henning Sprekeler, and Gustavo Deco. "Theory and simulation in neuroscience". In: *science* 338.6103 (2012), pp. 60–65. DOI: 10.1126/science.1227356.

[6] C Anthony Hunt et al. "At the biological modeling and simulation frontier". In: *Pharmaceutical research* 26.11 (2009), pp. 2369–2400. DOI: 10.1007/s11095-009-9958-3.

[7] Gaurang Mahajan and Suhita Nadkarni. "Intracellular calcium stores mediate metaplasticity at hippocampal dendritic spines". In: *The Journal of physiology* 597.13 (2019), pp. 3473–3502. DOI: 10.1113/JP277726.

[8] Jay S Coggan et al. "Evidence for ectopic neurotransmission at a neuronal synapse". In: *Science* 309.5733 (2005), pp. 446–451. DOI: 10.1126/science.1108239.

[9] Duncan E Donohue and Giorgio A Ascoli. "Automated reconstruction of neuronal morphology: an overview". In: *Brain research reviews* 67.1-2 (2011), pp. 94–102. DOI: 10.1016/j.brainresrev.2010.11.003.

[10] Marwan Abdellah. "In Silico Brain Imaging: Physically-plausible Methods for Visualizing Neocortical Microcircuitry". In: (2017), p. 400. DOI: 10.5075/epfl-thesis-8161. URL: http://infoscience.epfl.ch/record/232444.

[11] Corrado Cali et al. "3D cellular reconstruction of cortical glia and parenchymal morphometric analysis from Serial Block-Face Electron Microscopy of juvenile rat". In: *Progress in neurobiology* 183 (2019), p. 101696. DOI: 10.1016/j.pneurobio.2019.101696.

[12] Giorgio A Ascoli and Jeffrey L Krichmar. "L-Neuron: a modeling tool for the efficient generation and parsimonious description of dendritic morphology". In: *Neurocomputing* 32 (2000), pp. 1003–1011. DOI: 10.1016/S0925-2312(00)00272-1.

[13] Hermann Cuntz et al. "One rule to grow them all: a general theory of neuronal branching and its practical application". In: *PLoS computational biology* 6.8 (2010), e1000877. DOI: 10.1371/journal.pcbi.1000877.

[14] Lida Kanari et al. "Computational synthesis of cortical dendritic morphologies". In: *Cell Reports* 39.1 (2022), p. 110586. DOI: 10.1016/j.celrep.2022.110586.

[15] Eleftherios Zisis et al. "Digital Reconstruction of the Neuro-Glia-Vascular Architecture". In: *Cerebral Cortex* 31.12 (2021), pp. 5686–5703. DOI: 10.1093/cercor/bhab254.

[16] Giorgio A Ascoli, Duncan E Donohue, and Maryam Halavi. "NeuroMorpho. Org: a central resource for neuronal morphologies". In: *Journal of Neuroscience* 27.35 (2007), pp. 9247–9251.
DOI: 10.1523/JNEUROSCI.2055-07.2007.

[17] Pablo Blinder et al. "The cortical angiome: an interconnected vascular network with noncolumnar patterns of blood flow". In: *Nature neuroscience* 16.7 (2013), pp. 889–897.
DOI: 10.1038/nn.3426.

[18] Susan N Wright et al. "Digital reconstruction and morphometric analysis of human brain arterial vasculature from magnetic resonance angiography". In: *Neuroimage* 82 (2013), pp. 170–181.
DOI: 10.1016/j.neuroimage.2013.05.089.

[19] Marwan Abdellah et al. "NeuroMorphoVis: a collaborative framework for analysis and visualization of neuronal morphology skeletons reconstructed from microscopy stacks". In: *Bioinformatics* 34.13 (2018), pp. i574–i582.
DOI: 10.1093/bioinformatics/bty231.

[20] Michael L Hines and Nicholas T Carnevale. "The NEURON simulation environment". In: *Neural computation* 9.6 (1997), pp. 1179–1209.
DOI: 10.1162/neco.1997.9.6.1179.

[21] David A McCormick, Yousheng Shu, and Yuguo Yu. "Hodgkin and Huxley model—still standing?" In: *Nature* 445.7123 (2007), E1–E2.
DOI: 10.1038/nature05523.

[22] Johannes Reichold et al. "Vascular graph model to simulate the cerebral blood flow in realistic vascular networks". In: *Journal of Cerebral Blood Flow & Metabolism* 29.8 (2009), pp. 1429–1443.
DOI: 10.1038/jcbfm.2009.58.

[23] Bradley Feiger et al. "Determining the impacts of venoarterial extracorporeal membrane oxygenation on cerebral oxygenation using a one-dimensional blood flow simulator". In: *Journal of biomechanics* 104 (2020), p. 109707.
DOI: 10.1016/j.jbiomech.2020.109707.

[24] Marwan Abdellah et al. "Generating High Fidelity Surface Meshes of Neocortical Neurons using Skin Modifiers". In: *Computer Graphics and Visual Computing (CGVC)*. Ed. by Franck P. Vidal, Gary K. L. Tam, and Jonathan C. Roberts. The Eurographics Association, 2019. ISBN: 978-3-03868-096-3.
DOI: 10.2312/cgvc.20191257.

[25] Marwan Abdellah et al. "Metaball skinning of synthetic astroglial morphologies into realistic mesh models for visual analytics and in silico simulations". In: *Bioinformatics* 37.Supplement 1 (2021), pp. i426–i433.
DOI: 10.1093/bioinformatics/btab280.

[26] Marwan Abdellah et al. "Interactive visualization and analysis of morphological skeletons of brain vasculature networks with VessMorphoVis". In: *Bioinformatics* 36.Supplement 1 (2020), pp. i534–i541.
DOI: 10.1093/bioinformatics/btaa461.

[27] Joel R Stiles, Thomas M Bartol, et al. "Monte Carlo methods for simulating realistic synaptic microphysiology using MCell". In: *Computational neuroscience: realistic modeling for experimentalists* (2001), pp. 87–127.
DOI: 10.1201/9781420039290.ch4.

[28] Dawar Khan et al. "Molecular surface Remeshing with local region refinement". In: *International journal of molecular sciences* 19.5 (2018), p. 1383.
DOI: 10.3390/ijms19051383.

[29] Yixin Hu et al. "Tetrahedral meshing in the wild." In: *ACM Trans. Graph.* 37.4 (2018), pp. 60–1.
DOI: 10.1145/3386569.3392385.

[30] Xiaogai Li, Zhou Zhou, and Svein Kleiven. "An anatomically detailed and personalizable head injury model: significance of brain and white matter tract morphological variability on strain". In: *Biomechanics and modeling in mechanobiology* 20.2 (2021), pp. 403–431.
DOI: 10.1007/s10237-020-01391-8.

[31] Iain Hepburn et al. "STEPS: efficient simulation of stochastic reaction–diffusion models in realistic morphologies". In: *BMC systems biology* 6.1 (2012), pp. 1–19.
DOI: 10.1186/1752-0509-6-36.

[32] Steven S Andrews et al. "Detailed simulations of cell biology with Smoldyn 2.1". In: *PLoS Comput Biol* 6.3 (2010), e1000705.
DOI: 10.1371/journal.pcbi.1000705.

[33] Steven S Andrews. "Spatial and stochastic cellular modeling with the Smoldyn simulator". In: *Bacterial Molecular Networks*. Springer, 2012, pp. 519–542.
DOI: /10.1007/978-1-61779-361-5_26.

[34] Martin Robinson, Steven S Andrews, and Radek Erban. "Multiscale reaction-diffusion simulations with Smoldyn". In: *Bioinformatics* 31.14 (2015), pp. 2406–2408.
DOI: 10.1093/bioinformatics/btv149.

[35] Marwan Abdellah et al. "Physically-based in silico light sheet microscopy for visualizing fluorescent brain models". In: *BMC bioinformatics* 16.Suppl 11 (2015), S8.
DOI: 10.1186/1471-2105-16-S11-S8.

[36] Matt Pharr, Wenzel Jakob, and Greg Humphreys. *Physically based rendering: From theory to implementation*. Third edition. Morgan Kaufmann, 2016. ISBN: 0128006455. URL: http://pbrt.org.

[37] Hang Si. "TetGen, a Delaunay-based quality tetrahedral mesh generator". In: *ACM Transactions on Mathematical Software (TOMS)* 41.2 (2015), pp. 1–36.
DOI: 10.1145/2629697.

[38] François Labelle and Jonathan Richard Shewchuk. "Isosurface stuffing: fast tetrahedral meshes with good dihedral angles". In: *ACM SIGGRAPH 2007 papers*. 2007, 57–es.
DOI: 10.1145/1275808.1276448.

[39] Christophe Geuzaine and Jean-François Remacle. "Gmsh: A 3-D finite element mesh generator with built-in pre-and post-processing facilities". In: *International journal for numerical methods in engineering* 79.11 (2009), pp. 1309–1331.
DOI: 10.1002/nme.2579.

[40] Andreas Fabri and Sylvain Pion. "CGAL: The computational geometry algorithms library". In: *Proceedings of the 17th ACM SIGSPATIAL international conference on advances in geographic information systems*. 2009, pp. 538–539.
DOI: 10.1145/1653771.1653865.

[41] Yixin Hu et al. "Fast tetrahedral meshing in the wild". In: *ACM Transactions on Graphics (TOG)* 39.4 (2020), pp. 117–1.
DOI: 10.1145/3386569.3392385.

[42] Arunachalam Narayanaswamy et al. "Robust adaptive 3-D segmentation of vessel laminae from fluorescence confocal microscope images and parallel GPU implementation". In: *IEEE transactions on medical imaging* 29.3 (2009), pp. 583–597.
DOI: 10.1109/TMI.2009.2022086.

[43] Andrea Tagliasacchi et al. "Mean curvature skeletons". In: *Computer Graphics Forum*. Vol. 31. 5. Wiley Online Library. 2012, pp. 1735–1744.
DOI: 10.1111/j.1467-8659.2012.03178.x.

[44] Rafat Damseh et al. "Automatic graph-based modeling of brain microvessels captured with two-photon microscopy". In: *IEEE journal of biomedical and health informatics* 23.6 (2018), pp. 2551–2562.
DOI: 10.1109/JBHI.2018.2884678.

[45] Michał Januszewski et al. "High-precision automated reconstruction of neurons with flood-filling networks". In: *Nature methods* 15.8 (2018), pp. 605–610.
DOI: 10.1038/s41592-018-0049-4.

[46] J Alexander Bae et al. "Functional connectomics spanning multiple areas of mouse visual cortex". In: *bioRxiv* (2021).
DOI: 10.1101/2021.07.28.454025.

[47] Zhihao Zheng et al. "A complete electron microscopy volume of the brain of adult Drosophila melanogaster". In: *Cell* 174.3 (2018), pp. 730–743.
DOI: 10.1016/j.cell.2018.06.019.

[48] C Shan Xu et al. "A connectome of the adult drosophila central brain". In: *BioRxiv* (2020).
DOI: 10.1101/2020.01.21.911859.

[49] Sven Dorkenwald et al. "FlyWire: online community for whole-brain connectomics". In: *Nature methods* 19.1 (2022), pp. 119–128.
DOI: 10.1038/s41592-021-01330-0.

[50] Christopher T Lee et al. "An open-source mesh generation platform for biophysical modeling using realistic cellular geometries". In: *Biophysical journal* 118.5 (2020), pp. 1003–1008.
DOI: 10.1016/j.bpj.2019.11.3400.

[51] Jay S Coggan et al. "A Process for Digitizing and Simulating Biologically Realistic Oligocellular Networks Demonstrated for the Neuro-Glio-Vascular Ensemble". In: *Frontiers in neuroscience* 12 (2018).
DOI: 10.3389/fnins.2018.00664.

[52] Stefan Wils and Erik De Schutter. "STEPS: modeling and simulating complex reaction-diffusion systems with Python". In: *Frontiers in neuroinformatics* 3 (2009), p. 15.
DOI: 10.3389/neuro.11.015.2009.

[53] Weiliang Chen and Erik De Schutter. "Parallel STEPS: large scale stochastic spatial reaction-diffusion simulation with high performance computers". In: *Frontiers in Neuroinformatics* 11 (2017), p. 13.
DOI: 10.3389/fninf.2017.00013.

[54] Jay S Coggan et al. "Physiological dynamics in demyelinating diseases: unraveling complex relationships through computer modeling". In: *International journal of molecular sciences* 16.9 (2015), pp. 21215–21236.
DOI: 10.3390/ijms160921215.

[55] Giorgio A Ascoli et al. "Win–win data sharing in neuroscience". In: *Nature methods* 14.2 (2017), pp. 112–116.
DOI: 10.1038/nmeth.4152.

[56] Shin-ya Takemura et al. "Synaptic circuits and their variations within different columns in the visual system of Drosophila". In: *Proceedings of the National Academy of Sciences* 112.44 (2015), pp. 13711–13716.

[57] Narayanan Kasthuri et al. "Saturated reconstruction of a volume of neocortex". In: *Cell* 162.3 (2015), pp. 648–661.
DOI: 10.1016/j.cell.2015.06.054.

[58] Sven Dorkenwald et al. "Automated synaptic connectivity inference for volume electron microscopy". In: *Nature methods* 14.4 (2017), pp. 435–442.
DOI: 10.1038/nmeth.4206.

[59] Stephan Grein et al. "1D-3D hybrid modeling—from multi-compartment models to full resolution models in space and time". In: *Frontiers in neuroinformatics* 8 (2014), p. 68.

[60] Sébastien Lasserre et al. "A neuron membrane mesh representation for visualization of electrophysiological simulations". In: *IEEE Transactions on Visualization and Computer Graphics* 18.2 (2012), pp. 214–227. DOI: 10.1109/TVCG.2011.55.

[61] Juan P Brito et al. "Neuronize: a tool for building realistic neuronal cell morphologies". In: *Frontiers in neuroanatomy* 7 (2013). DOI: 10.3389/fnana.2013.00015.

[62] Juan J Garcia-Cantero et al. "NeurotessMesh: A tool for the Generation and Visualization of Neuron Meshes and Adaptive on-the-Fly Refinement". In: *Frontiers in neuroinformatics* 11 (2017), p. 38. DOI: 10.3389/fninf.2017.00038.

[63] Robert A McDougal, Michael L Hines, and William W Lytton. "Water-tight membranes from neuronal morphology files". In: *Journal of neuroscience methods* 220.2 (2013), pp. 167–178. DOI: 10.1016/j.jneumeth.2013.09.011.

[64] Konstantin Mörschel, Markus Breit, and Gillian Queisser. "Generating neuron geometries for detailed three-dimensional simulations using anamorph". In: *Neuroinformatics* 15.3 (2017), pp. 247–269. DOI: 10.1007/s12021-017-9329-x.

[65] Robert A McDougal and Gordon M Shepherd. "3D-printer visualization of neuron models". In: *Frontiers in neuroinformatics* 9 (2015), p. 18. DOI: 10.3389/fninf.2015.00018.

[66] Kenny Erleben et al. *Physics-based animation*. Charles River Media Hingham, 2005.

[67] Srikanth Ramaswamy et al. "The neocortical microcircuit collaboration portal: a resource for rat somatosensory cortex". In: *Frontiers in neural circuits* 9 (2015). DOI: 10.3389/fncir.2015.00044.

[68] Franca Schmid et al. "Vascular density and distribution in neocortex". In: *Neuroimage* 197 (2019), pp. 792–805. DOI: 10.1016/j.neuroimage.2017.06.046.

[69] Samuel A Mihelic et al. "Segmentation-Less, Automated, Vascular Vectorization". In: *PLoS computational biology* 17.10 (2021), e1009451. DOI: 10.1371/journal.pcbi.1009451.

[70] Kwanghun Chung and Karl Deisseroth. "CLARITY for mapping the nervous system". In: *Nat Meth* 10.6 (June 2013), pp. 508–513. DOI: 10.1038/nmeth.2481.

[71] Yi Feng et al. "CLARITY reveals dynamics of ovarian follicular architecture and vasculature in three-dimensions". In: *Scientific Reports* 7.1 (2017), pp. 1–13. DOI: 10.1038/srep44810.

[72] Antonino Paolo Di Giovanna et al. "Whole-brain vasculature reconstruction at the single capillary level". In: *Scientific reports* 8.1 (2018), pp. 1–11. DOI: 10.1038/s41598-018-30533-3.

[73] Takeyuki Miyawaki et al. "Visualization and molecular characterization of whole-brain vascular networks with capillary resolution". In: *Nature communications* 11.1 (2020), pp. 1–11. DOI: 10.1038/s41467-020-14786-z.

[74] Marwan Abdellah et al. "Physically-based rendering of highly scattering fluorescent solutions using path tracing". In: *Proceedings of the 37th Annual Conference of the European Association for Computer Graphics: Posters*. Eurographics Association. 2016, pp. 17–18.
DOI: 10.2312/egp.20161045.

[75] Mehdi Azimipour et al. "Extraction of optical properties and prediction of light distribution in rat brain tissue". In: *Journal of Biomedical Optics* 19.7 (2014).
DOI: 10.1117/1.JBO.19.7.075001.

[76] Rohit Chandra. *Parallel programming in OpenMP*. Morgan kaufmann, 2001. ISBN: 9780262533027.

List of Figures

1 **Ultraliser workflow.** Ultraliser implements a voxelization-based engine to create annotated volume models and watertight surface manifolds from input morphology skeletons, non-watertight triangular soups, gray scale volumes and segmented binary masks. 23

2 **Ultraliser creates high-fidelity watertight surface manifolds of neuropil structures from non-watertight inputs.** (**a**) The EM volume block is segmented semi-automatically to extract 3D mesh models of individual cell morphologies and other structures (Supplementary Fig. S3). (**b**) An exemplar mesh (Astrocyte 4) is selected for evaluating the optimum values of the remeshing parameters. (**c**) The effect of varying voxelization resolution (in voxels per micron) and the number of optimization iterations on—from left to right—the Hausdorff distance (in μm), number of vertices, total surface area (in μm^2) and volume (μm^3) of the mesh. Astrocyte 4 has been re-meshed at multiple voxelization resolutions (0.1 - 1.0 μm) and optimized with different optimization iterations (1 - 10) to determine the most optimum values for these parameters as a reference to be used to remesh all the other segmented structures from the neuropil volume. (**d**) The input mesh of Astrocyte 4 is not watertight and is also over tessellated with ∼1.7 million triangles. This mesh has been re-meshed with a voxelization resolution of 5 voxels per micron (200 nm), and optimized with one, five and ten optimization iterations. (**e**) ultraMesh2Mesh creates an adaptively optimized watertight mesh with only ∼425 thousand triangles. The distributions show a comparison between the qualitative analysis metrics of the input mesh and resulting one. Scale bars, 5μm (**b**), 2.5μm (**d**). 24

3 **Remeshing fragmented mesh model with multiple mesh partitions, thousands of self intersecting faces and slicing artifacts.** (**a**) Segmented mesh model of a neuron extracted from layer II/III of the visual cortex of the rat. The closeup in (b) shows the messy fragmented structure of the mesh. This triangle soup has been processed with Ultraliser to generate an optimized, connected and two-manifold mesh model with high quality topology at three different resolutions: (**c**) one, (**d**) five and (**e**) 10 voxels per micron. The closeups in (**f**) - (**i**) focus on a small spiny branch to highlight the effect of varying the reconstruction resolution on the ultrastructure of the mesh. Supplementary Fig. S55 shows comparative analysis between the input mesh and the ultralised one. (**j**) The mesh contains a few gaps due to the misalignment and slicing artifacts. The 3-way solid voxelization is used to reconstruct a continuous manifold with optimized topology at different resolutions (**k, l, m**). Scale bars, 10 μm (**a**), 5 μm (**b, c, d, e**), 1 μm (**f, g, h, i**). 25

4 **Creating biologically realistic spiny neuronal surface mesh from its morphology.** (**a**) Progressive reconstruction of the soma from an initial icosphere into a 3D plausible profile based on the FEM approach[66]. (**b**) The morphology is rendered as a set of samples. (**c**) For each neurite, we reconstruct a list of proxy-geometries linking a set of principal sections from the root node and until the leaf: level 1 is in red, level 2 is in green, and level 3 is in blue. Note that the proxy geometries start from the origin of the soma to avoid any gaps when the soma mesh is added afterwards (**d**). (**e**) Spine proxy geometries are added along the surface of the proxy-mesh. All the section geometries, spines and somatic mesh are rasterized to create a continuous and watertight manifold. Renderings of multiple closeups of this mesh are shown in Supplementary Figure S80. Scale bars, 5 μm (**a**) and 20 μm (**b, c, d, e**). 26

5 **Reconstruction of a watertight mesh of a cerebral vascular network from its corresponding vectorized graph.** (a) The data set is sliced from a larger cortical network with hundreds of millions of vertices to demonstrate how Ultraliser is effective in building mesh models with clean geometric topology and accurate branching structures from raw vectorized morphologies. (b) The data set is qualitatively and quantitatively analyzed to evaluate its local geometry and topology (Supplementary Table S8). (c) A closeup revealing the overlap between the different sections at a common branching point, where each section is assigned a different color based on its average radius. (d) Each section of morphology is converted into a tubular proxy mesh with a circular cross-section interpolated at every vertex along the section. (e) We add packing spheres (in yellow) at the terminal samples of each section to ensure the smoothness and continuity of the proxy mesh. (f) The proxy mesh is rasterized into a volumetric grid with a resolution of five microns per voxel, where the overlap between the different sections is obvious. (g) Applying the 3-way solid voxelization algorithm fills the intravascular space and removes any intersections, in which we can extract a continuous manifold of every partition in the volume. (h) A watertight mesh is reconstructed with clean geometric topology and accurate branching. This mesh can be then used in several simulation experiments. Scale bars, 100 μm (**a**), 50 μm (**c**$_1$, **d**$_1$, **e**$_1$, **f**$_1$, **g**$_1$, **h**$_1$), 25 μm (**c**$_2$, **d**$_2$, **e**$_2$, **f**$_2$, **g**$_2$, **h**$_2$). 27

6 **Creating annotated volumetric tissue models for *in silico* imaging.** (a) The mesh is created using NeuroMorphoVis[19] from a neuronal morphology reconstructed from the somatosensory cortex of a P14 rat[67]. (b) The neuron is placed into a digital circuit[2] to determine its connectivity in which we can identify the synaptic locations and integrate the spines along its dendritic arborizations. (b) The neuron mesh is used to reconstruct a high resolution annotated volume in which its intracellular space is tagged with optical properties of multiple fluorescent dyes. The volume is then used for simulating the imaging of a single cell with fluorescence microscope. The following dyes are used Alexa Fluor 488, 405, 532, 658 and 610 in (c), (d$_1$), (d$_2$), (d$_3$) and (d$_4$) respectively. The simulated tissue block is illuminated with collimated laser beams at a wavelength that corresponds to the maximum excitation of each respective dye. (e) *In silico* brainbow optical section of a digitally reconstructed neocortical slice (920 $\times$ 640 $\times$ 1740 cubic microns) simulating the imaging of lightsheet fluorescence microscope. The slice is tagged with six fluorescent labels (GFP, CFP, eCFP, mBannan, mCheery and mPlum) and illuminated at the maximum excitation wavelength of each respective dye. Scale bars 25 μm (**a-d**), 50 μm (**e**). 28

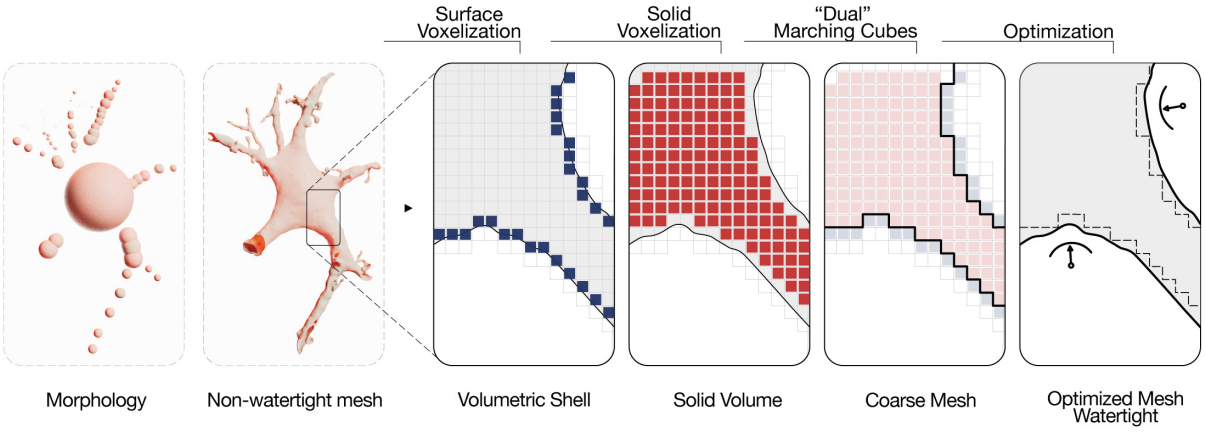

Figure 1 | Ultraliser workflow.
Ultraliser implements a voxelization-based engine to create annotated volume models and watertight surface manifolds from input morphology skeletons, non-watertight triangular soups, gray scale volumes and segmented binary masks.

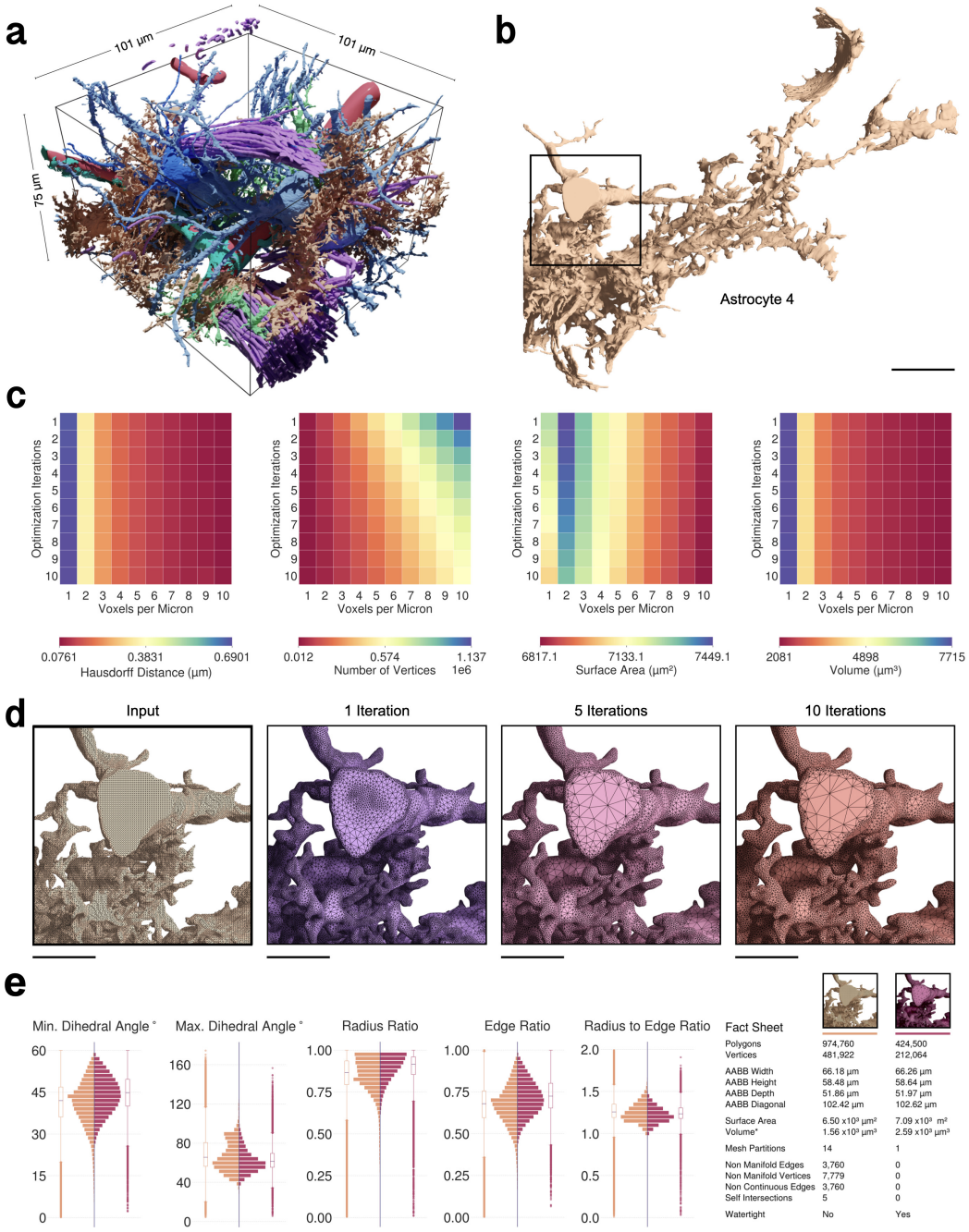

Figure 2 | Ultraliser creates high-fidelity watertight surface manifolds of neuropil structures from non-watertight inputs. (**a**) The EM volume block is segmented semi-automatically to extract 3D mesh models of individual cell morphologies and other structures (Supplementary Fig. S3). (**b**) An exemplar mesh (Astrocyte 4) is selected for evaluating the optimum values of the remeshing parameters. (**c**) The effect of varying voxelization resolution (in voxels per micron) and the number of optimization iterations on—from left to right—the Hausdorff distance (in µm), number of vertices, total surface area (in μm^2) and volume (μm^3) of the mesh. Astrocyte 4 has been re-meshed at multiple voxelization resolutions (0.1 - 1.0 µm) and optimized with different optimization iterations (1 - 10) to determine the most optimum values for these parameters as a reference to be used to remesh all the other segmented structures from the neuropil volume. (**d**) The input mesh of Astrocyte 4 is not watertight and is also over tessellated with ∼1.7 million triangles. This mesh has been re-meshed with a voxelization resolution of 5 voxels per micron (200 nm), and optimized with one, five and ten optimization iterations. (**e**) ULTRAMESH2MESH creates an adaptively optimized watertight mesh with only ∼425 thousand triangles. The distributions show a comparison between the qualitative analysis metrics of the input mesh and resulting one.
Scale bars, 5μm (**b**), 2.5μm (**d**).

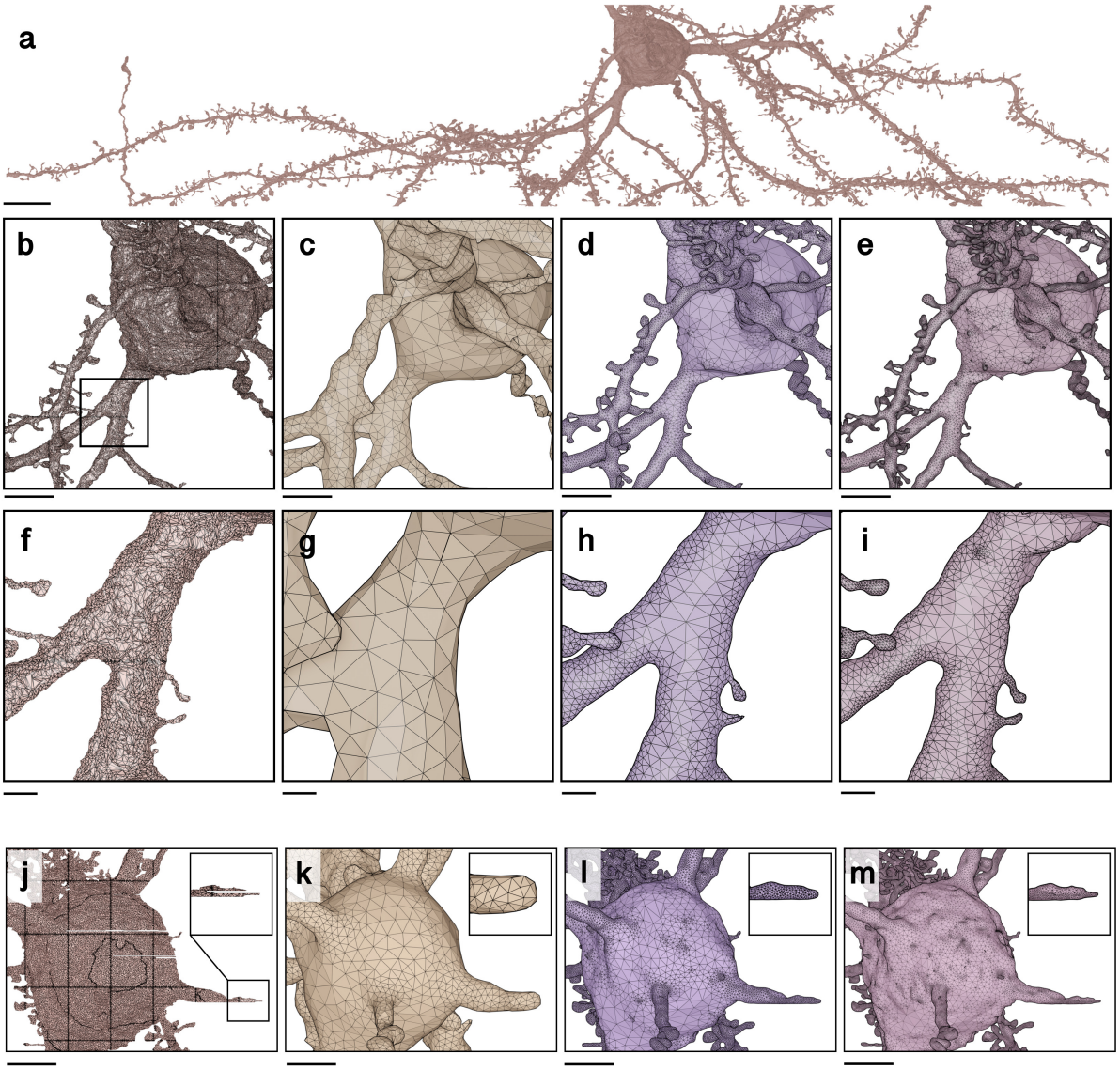

Figure 3 | Remeshing fragmented mesh model with multiple mesh partitions, thousands of self intersecting faces and slicing artifacts.
(**a**) Segmented mesh model of a neuron extracted from layer II/III of the visual cortex of the rat. The closeup in (b) shows the messy fragmented structure of the mesh. This triangle soup has been processed with Ultraliser to generate an optimized, connected and two-manifold mesh model with high quality topology at three different resolutions: (**c**) one, (**d**) five and (**e**) 10 voxels per micron. The closeups in (**f**) - (**i**) focus on a small spiny branch to highlight the effect of varying the reconstruction resolution on the ultrastructure of the mesh. Supplementary Fig. S55 shows comparative analysis between the input mesh and the ultralised one. (**j**) The mesh contains a few gaps due to the misalignment and slicing artifacts. The 3-way solid voxelization is used to reconstruct a continuous manifold with optimized topology at different resolutions (**k, l, m**).
Scale bars, 10 μm (**a**), 5 μm (**b, c, d, e**), 1 μm (**f, g, h, i**).

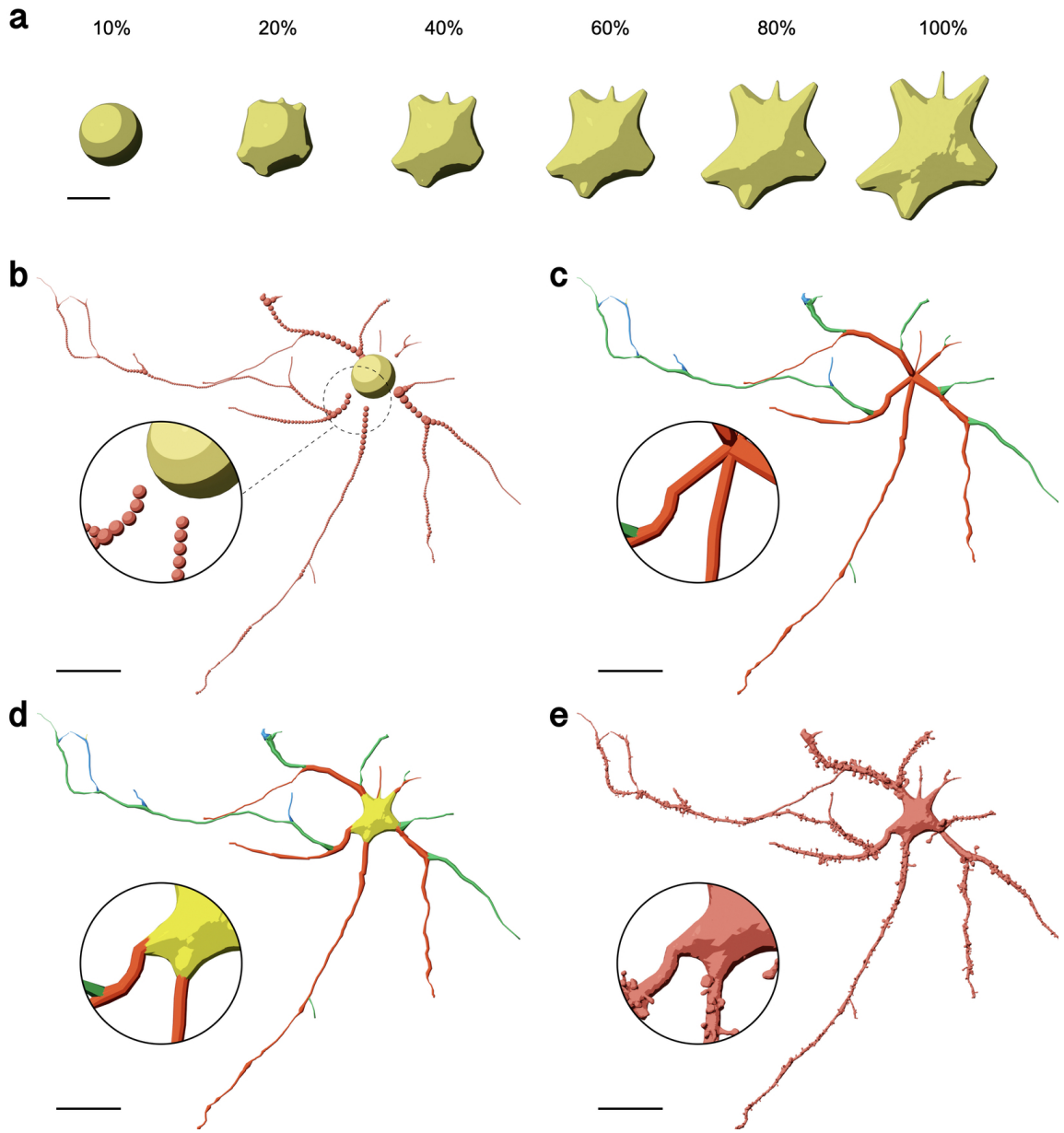

Figure 4 | Creating biologically realistic spiny neuronal surface mesh from its morphology.
(**a**) Progressive reconstruction of the soma from an initial icosphere into a 3D plausible profile based on the FEM approach[66]. (**b**) The morphology is rendered as a set of samples. (**c**) For each neurite, we reconstruct a list of proxy-geometries linking a set of principal sections from the root node and until the leaf: level 1 is in red, level 2 is in green, and level 3 is in blue. Note that the proxy geometries start from the origin of the soma to avoid any gaps when the soma mesh is added afterwards (**d**). (**e**) Spine proxy geometries are added along the surface of the proxy-mesh. All the section geometries, spines and somatic mesh are rasterized to create a continuous and watertight manifold. Renderings of multiple closeups of this mesh are shown in Supplementary Figure S80.
Scale bars, 5 μm (**a**) and 20 μm (**b, c, d, e**).

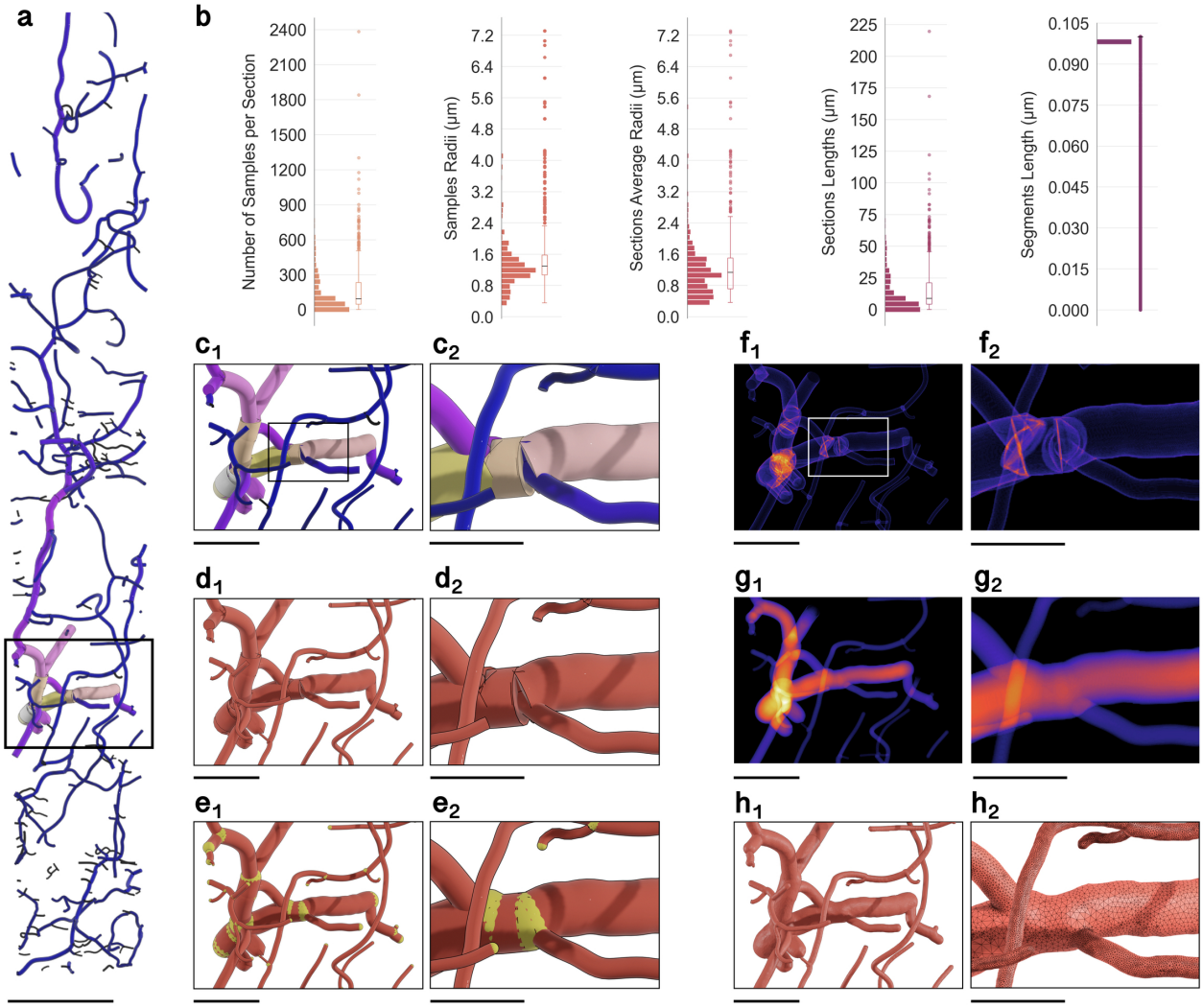

Figure 5 | Reconstruction of a watertight mesh of a cerebral vascular network from its corresponding vectorized graph. (a) The data set is sliced from a larger cortical network with hundreds of millions of vertices to demonstrate how Ultraliser is effective in building mesh models with clean geometric topology and accurate branching structures from raw vectorized morphologies. (b) The data set is qualitatively and quantitatively analyzed to evaluate its local geometry and topology (Supplementary Table S8). (c) A closeup revealing the overlap between the different sections at a common branching point, where each section is assigned a different color based on its average radius. (d) Each section of morphology is converted into a tubular proxy mesh with a circular cross-section interpolated at every vertex along the section. (e) We add packing spheres (in yellow) at the terminal samples of each section to ensure the smoothness and continuity of the proxy mesh. (f) The proxy mesh is rasterized into a volumetric grid with a resolution of five microns per voxel, where the overlap between the different sections is obvious. (g) Applying the 3-way solid voxelization algorithm fills the intravascular space and removes any intersections, in which we can extract a continuous manifold of every partition in the volume. (h) A watertight mesh is reconstructed with clean geometric topology and accurate branching. This mesh can be then used in several simulation experiments. Scale bars, 100 μm (**a**), 50 μm (**c**$_1$, **d**$_1$, **e**$_1$, **f**$_1$, **g**$_1$, **h**$_1$), 25 μm (**c**$_2$, **d**$_2$, **e**$_2$, **f**$_2$, **g**$_2$, **h**$_2$).

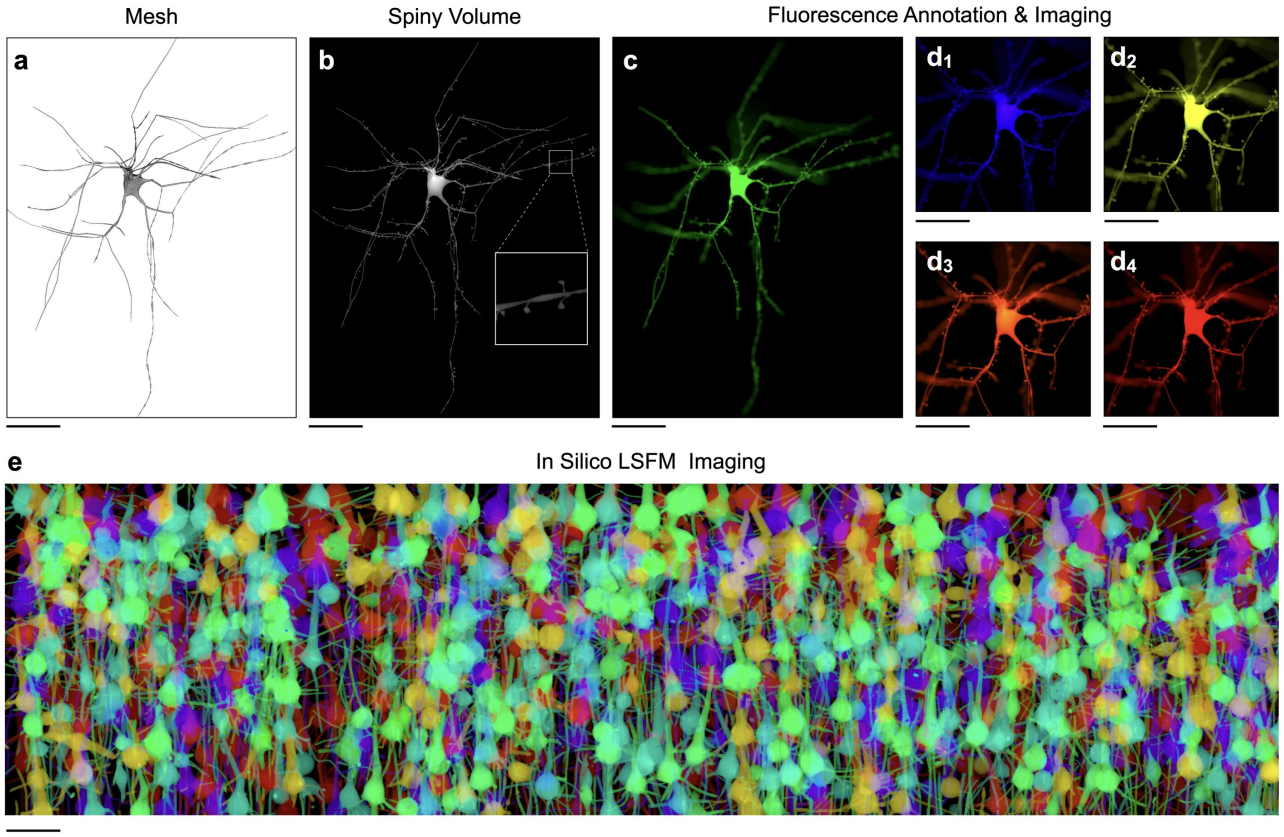

Figure 6 | Creating annotated volumetric tissue models for *in silico* imaging.
(a) The mesh is created using NeuroMorphoVis[19] from a neuronal morphology reconstructed from the somatosensory cortex of a P14 rat[67]. (b) The neuron is placed into a digital circuit[2] to determine its connectivity in which we can identify the synaptic locations and integrate the spines along its dendritic arborizations. (b) The neuron mesh is used to reconstruct a high resolution annotated volume in which its intracellular space is tagged with optical properties of multiple fluorescent dyes. The volume is then used for simulating the imaging of a single cell with fluorescence microscope. The following dyes are used Alexa Fluor 488, 405, 532, 658 and 610 in (c), (d_1), (d_2), (d_3) and (d_4) respectively. The simulated tissue block is illuminated with collimated laser beams at a wavelength that corresponds to the maximum excitation of each respective dye. (e) *In silico* brainbow optical section of a digitally reconstructed neocortical slice (920 × 640 × 1740 cubic microns) simulating the imaging of lightsheet fluorescence microscope. The slice is tagged with six fluorescent labels (GFP, CFP, eCFP, mBannan, mCheery and mPlum) and illuminated at the maximum excitation wavelength of each respective dye.
Scale bars 25 μm (**a-d**), 50 μm (**e**).